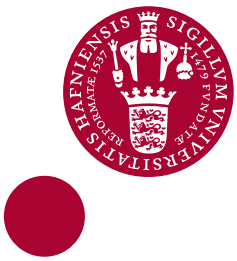

# Systems-wide Analysis of Serine ADP-Ribosylation Reveals Widespread Occurrence and Site-Specific Overlap with Phosphorylation

Larsen, Sara C.; Hendriks, Ivo A.; Lyon, David; Jensen, Lars J.; Nielsen, Michael L.

*Published in:*
Cell Reports

*DOI:*
10.1016/j.celrep.2018.07.083

*Publication date:*
2018

*Document version*
Publisher's PDF, also known as Version of record

Resource

Cell Reports

# Systems-wide Analysis of Serine ADP-Ribosylation Reveals Widespread Occurrence and Site-Specific Overlap with Phosphorylation

## Graphical Abstract

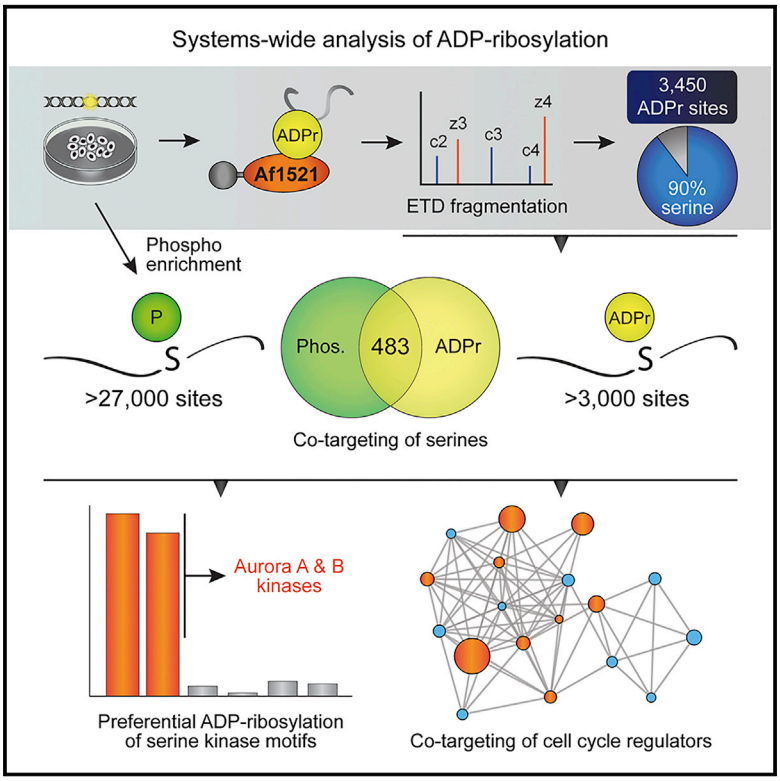


## Highlights

- Proteome-wide analysis pinpoints 3,450 ADP-ribosylation sites with confidence
- ADP-ribosylation predominantly targets serine residues in response to oxidative stress
- Phosphoproteomics demonstrate co-targeting of ADP-ribosylation and phosphorylation
- PARP enzymes and Aurora kinases preferentially modify the same serine residues

## Authors

Sara C. Larsen, Ivo A. Hendriks, David Lyon, Lars J. Jensen, Michael L. Nielsen

## Correspondence

michael.lund.nielsen@cpr.ku.dk

## In Brief

By combining unbiased proteomics analyses with unrestricted data processing, Larsen et al. demonstrate that serine residues are the primary target of system-wide ADP-ribosylation in response to oxidative stress. Moreover, the authors show that a significant degree of serine residues are co-targeted by ADP-ribosylation and phosphorylation in the DNA damage response.

Larsen et al., 2018, Cell Reports *24*, 2493–2505
August 28, 2018 
https://doi.org/10.1016/j.celrep.2018.07.083

CellPress

Cell Reports
Resource



# Systems-wide Analysis of Serine ADP-Ribosylation Reveals Widespread Occurrence and Site-Specific Overlap with Phosphorylation

Sara C. Larsen,[1,3] Ivo A. Hendriks,[1,3] David Lyon,[2] Lars J. Jensen,[2] and Michael L. Nielsen[1,4,*]
[1]Proteomics Program, Novo Nordisk Foundation Center for Protein Research, Faculty of Health and Medical Sciences, University of Copenhagen, Blegdamsvej 3B, 2200 Copenhagen, Denmark
[2]Disease Systems Program, Novo Nordisk Foundation Center for Protein Research, Faculty of Health and Medical Sciences, University of Copenhagen, Blegdamsvej 3B, 2200 Copenhagen, Denmark
[3]These authors contributed equally
[4]Lead Contact
*Correspondence: michael.lund.nielsen@cpr.ku.dk
https://doi.org/10.1016/j.celrep.2018.07.083

## SUMMARY

**ADP-ribosylation (ADPr) is a reversible posttranslational modification involved in a range of cellular processes. Here, we report system-wide identification of serine ADPr in human cells upon oxidative stress. High-resolution mass spectrometry and unrestricted data processing confirm that serine residues are the major target of ADPr in HeLa cells. Proteome-wide analysis identifies 3,090 serine ADPr sites, with 97% of acceptor sites modulating more than 2-fold upon oxidative stress, while treatment with the poly (ADP-ribose) polymerase (PARP) inhibitor olaparib abrogates this induction. Serine ADPr predominantly targets nuclear proteins, while structural-predictive analyses reveal that serine ADPr preferentially targets disordered protein regions. The identified ADP-ribosylated serines significantly overlap with known phosphorylated serines, and large-scale phosphoproteomics analysis provides evidence for site-specific crosstalk between serine ADPr and phosphorylation. Collectively, we demonstrate that serine ADPr is a widespread modification and a major nuclear signaling response to oxidative stress, with a regulatory scope comparable to other extensive posttranslational modifications.**

## INTRODUCTION

ADP-ribosylation is a posttranslational modification (PTM) in which an ADP-ribose moiety is transferred from NAD+ to the amino acid side chain of target proteins (Ueda and Hayaishi, 1985), thereby altering the function of the modified protein, providing a regulatory mechanism for protein-protein interactions, or regulating protein localization (Hottiger, 2015; Jungmichel et al., 2013; Seman et al., 2004). The modification entails either the addition of a single mono-ADP-ribose, referred to as mono-ADP-ribosylation (MAR), or the addition to an already protein-bound ADP-ribose to form poly-ADP-ribosylation (PAR) (Schreiber et al., 2006). ADP-ribosylation (ADPr) is catalyzed by a class of enzymes known as ADP-ribosyltransferases (ARTs), which can be divided into two major subclasses, ARTCs (cholera toxin-like, also known as ecto-ARTs) and ARTDs (diphtheria toxin-like, formerly called PARPs [poly (ADP-ribose) polymerases]), depending on their conserved structural features (Hottiger et al., 2010). ARTDs/PARPs are known as crucial enzymes in biological processes related to cancer development (Gibson and Kraus, 2012; Schreiber et al., 2006), with PARP inhibitors emerging as promising anticancer agents and commonly used in the clinic for treatment of ovarian and breast cancer (Lord and Ashworth, 2017; Pommier et al., 2016; Rouleau et al., 2010).

Within mammalian cells, ADPr can enzymatically be attached to several amino acid residues, including Glu, Asp, Lys, Asn, His, Arg, Cys, and Ser (Leung, 2017). Recently, western blot analyses revealed that serine residues are a major ADPr target during DNA damage (Palazzo et al., 2018). Serine ADPr is catalyzed by ARTD1/PARP1 and ARTD2/PARP2 and requires the co-factor histone PARylation factor 1 (HPF1) to attach ADP-ribose groups onto the side chain of serine residues (Bonfiglio et al., 2017). Similar to most PTMs, serine ADPr is dynamic and can be enzymatically removed by the hydrolase ARH3 (Abplanalp et al., 2017; Fontana et al., 2017). Despite representing a major fraction of total ADPr after DNA damage in mammalian cells (Palazzo et al., 2018), identification of the proteins and individual serine ADPr acceptor sites still remains challenging. Initial investigations aimed at mapping serine residues carrying ADPr yielded 79 and 224 serine acceptor sites, respectively (Bilan et al., 2017; Bonfiglio et al., 2017). With hundreds of proteins globally known to be targeted by ADPr (Vivelo et al., 2017), we reasoned that the extent of serine ADPr is likely to be far greater than currently reported. Thus, to gain further insight into the serine ADP-ribosylome, we performed a system-wide analysis in HeLa cells using an augmented proteomics Af1521 enrichment strategy.

For confident mapping of the amino acid residues modified with ADPr, all enriched peptides were sequenced using high-resolution electron transfer dissociation (ETD) fragmentation (Coon

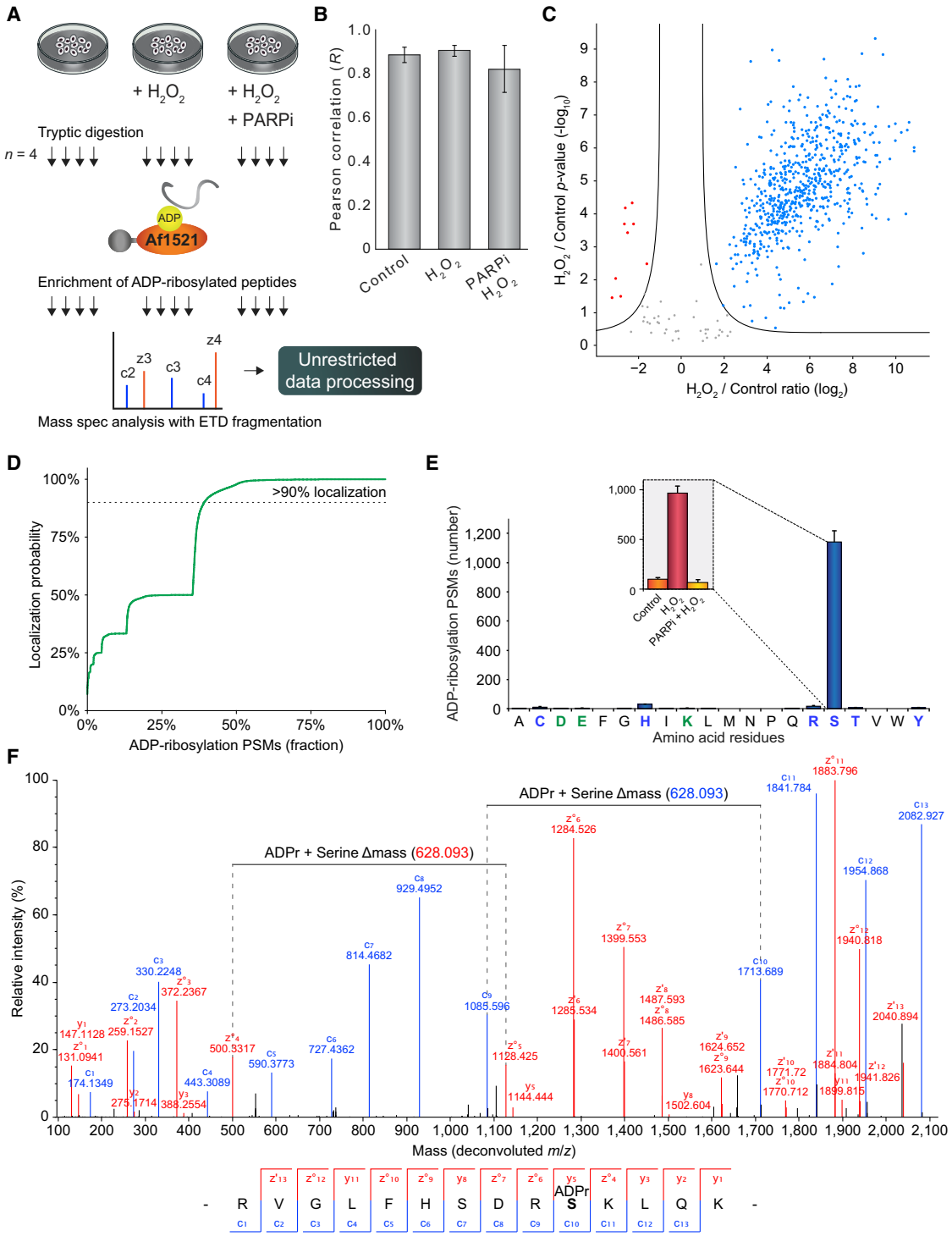


**Figure 1. Unbiased Localization of ADPr Acceptor Sites**

(A) Overview of the experimental design. Briefly, quadruplicate (n = 4) cultures of HeLa cells were subjected to the indicated treatments, after which tryptic digestion was performed, and subsequently ADPr peptides were enriched using the Af1521 macrodomain. All samples were analyzed by MS as single-shot analyses using electron transfer dissociation (ETD) fragmentation, followed by unrestricted data processing.

(B) Average Pearson correlation of identified ADPr peptides (localization probability >0.90) from the three conditions. Error bars represent SD.

(C) Volcano plot analysis to visualize ADPr dynamics in response to $H_2O_2$ treatment. Blue dots indicate upregulated proteins, and red dots indicate downregulated proteins.

*(legend continued on next page)*

et al., 2005) on an Orbitrap Fusion Lumos mass spectrometer (Senko et al., 2013), enabling proteome-wide mapping of ADPr sites to great depth and facilitating a high degree of localization confidence. Collectively, we identified 3,090 serine ADPr sites, hereby significantly extending current knowledge of serine ADPr while simultaneously providing insights into this emerging modification. Exemplifying this, we find that serine ADPr significantly overlaps with known phosphorylation sites. A systematic kinase-substrate network analysis hinted that serine residues usually modulated in phosphorylation by Aurora kinases were primarily targeted by ADPr upon oxidative stress. Thus, we provide insight into widespread and site-specific crosstalk between serine ADPr and serine phosphorylation. In conclusion, we present a prominent resource on the serine-specific ADP-ribosylome, demonstrating global and dominant increase in serine ADPr upon oxidative stress and pinpointing a great number of modified residues.

## RESULTS

### Unrestricted Analysis of Amino Acids Targeted by ADPr

With ADPr reported to target a wide range of amino acid residues (Glu, Asp, Lys, Arg, His, Cys, and Ser) (Gupte et al., 2017), we wanted to assess the capability of our proteomics strategy to confidently localize ADPr. Therefore, we compared higher-energy collisional dissociation (HCD) fragmentation with the ETD fragmentation. In contrast to HCD, ETD fragmentation is achieved by transferring electrons to the multiply charged cations, thereby introducing fragmentation randomly along the peptide backbone in a sequence independent manner (Syka et al., 2004). This makes ETD particularly useful for analysis of labile modifications such as phosphorylation (Molina et al., 2007) and ADPr (Zee and Garcia, 2010).

For comparison between HCD and ETD fragmentation, small-scale quadruplicate HeLa cell cultures were treated with $H_2O_2$, and ADPr peptides were purified using the Af1521 macrodomain (Martello et al., 2016) and subsequently analyzed using either HCD or ETD fragmentation. To assess the ability of HCD and ETD for unbiased and confident localization of ADPr, an unrestricted search of the mass spectrometry (MS) data was performed, by allowing the ADPr moiety to reside *in silico* on any of the 20 naturally occurring amino acids.

Overall, we observed that the largest number of ADPr peptides were identified and localized with ETD fragmentation in combination with detection of peptides in the Orbitrap mass analyzer (Figure S1A). Compared to the Orbitrap mass analyzer, the poor resolution of the ion trap more frequently resulted in a failure to faithfully identify and localize ADPr. Surprisingly, whereas HCD analysis resulted in a considerably larger number of MS/MS scans, only a very small fraction of these scans (<1%) could be confidently localized when using a fully unrestricted search (Figure S1B). Collectively, this demonstrated the analytical superiority of ETD fragmentation for confident localization of ADPr.

To obtain an unbiased assessment of amino acids modified with ADPr and assess the effect of oxidative stress on the distribution of modified amino acids, we performed quadruplicate experiments in HeLa cells either mock treated or exposed to $H_2O_2$ in the presence or absence of the PARP inhibitor olaparib (Figure 1A). In this experiment, ADPr peptides were enriched using our established Af1521 enrichment approach (Martello et al., 2016) and subsequently analyzed by single-shot MS. We obtained a high degree of reproducibility between our experimental replicates (Figures 1B and S1C), which facilitated reliable quantification of the analyzed samples using label-free quantification (LFQ) (Cox et al., 2014). In response to $H_2O_2$ treatment, we observed a substantial increase in ADPr peptides, with the majority of ADPr events being upregulated more than 2-fold (Figure 1C). Conversely, the induction was entirely abrogated when treating cells with the PARP inhibitor olaparib prior to oxidative stress (Wahlberg et al., 2012) (Figure S1D).

Acquired MS/MS spectra were searched using our unrestricted approach, with assignment solely based upon high-resolution ETD data, thus unconditionally relying on the non-ergodic fragmentation propensity entailed in the acquired ETD MS/MS spectra for determination of ADPr acceptor sites (Zubarev et al., 1998). From our unrestricted data processing, we obtained confident localization of ADPr within modified peptides, with 1,297 ADPr sites identified and localized at a probability of >90% (Figure 1D). 1,204 of the 1,297 (93%) ADPr sites confidently localized to serine residues (Figure 1E).

Our finding substantiates initial observations that serines are prominent targets of ADPr in human cells (Leidecker et al., 2016; Palazzo et al., 2018) while providing quantitative and site-specific insight into the cellular prevalence of the modification during oxidative stress (Figure 1E). Upon oxidative stress, predominantly serine ADPr sites were modulated, while treatment of cells with PARP inhibitor (olaparib) abrogated their stress-induced regulation (Figures 1E and S1E). Notably, our ETD analysis demonstrated prodigious fragmentation spectra of serine ADPr peptides, providing unambiguous localization of the modified residue (Figure 1F). Having established a strategy for studying serine ADPr, we next sought to investigate the cellular extent of the modification in more detail.

### Mapping the Serine ADP-Ribosylome

To gain comprehensive coverage of the serine ADP-ribosylome, we combined our Af1521 enrichment strategy with previously

(D) Localization probability distribution of identified ADPr peptide-spectrum matches (PSMs). The dashed line visualizes the cutoff of >90% localization probability that we used for filtering our data.

(E) Histogram depicting the distribution of identified acceptor amino acid residues derived from unrestricted data processing of ETD data. Amino acid residues to which we confidently localized ADPr in quadruplicate are indicated in blue, and other previously reported ADP-ribosylated amino acid residues are indicated in green. Inset: regulation of serine ADPr upon $H_2O_2$ and PARP inhibition. Error bars represent SD.

(F) Fully annotated representative ETD tandem mass spectrum of an ADP-ribosylated peptide. Full fragmentation is obtained, with both c-ions (blue) and z-ions (red) pinpointing the ADPr to reside on a serine residue.

See also Figure S1.

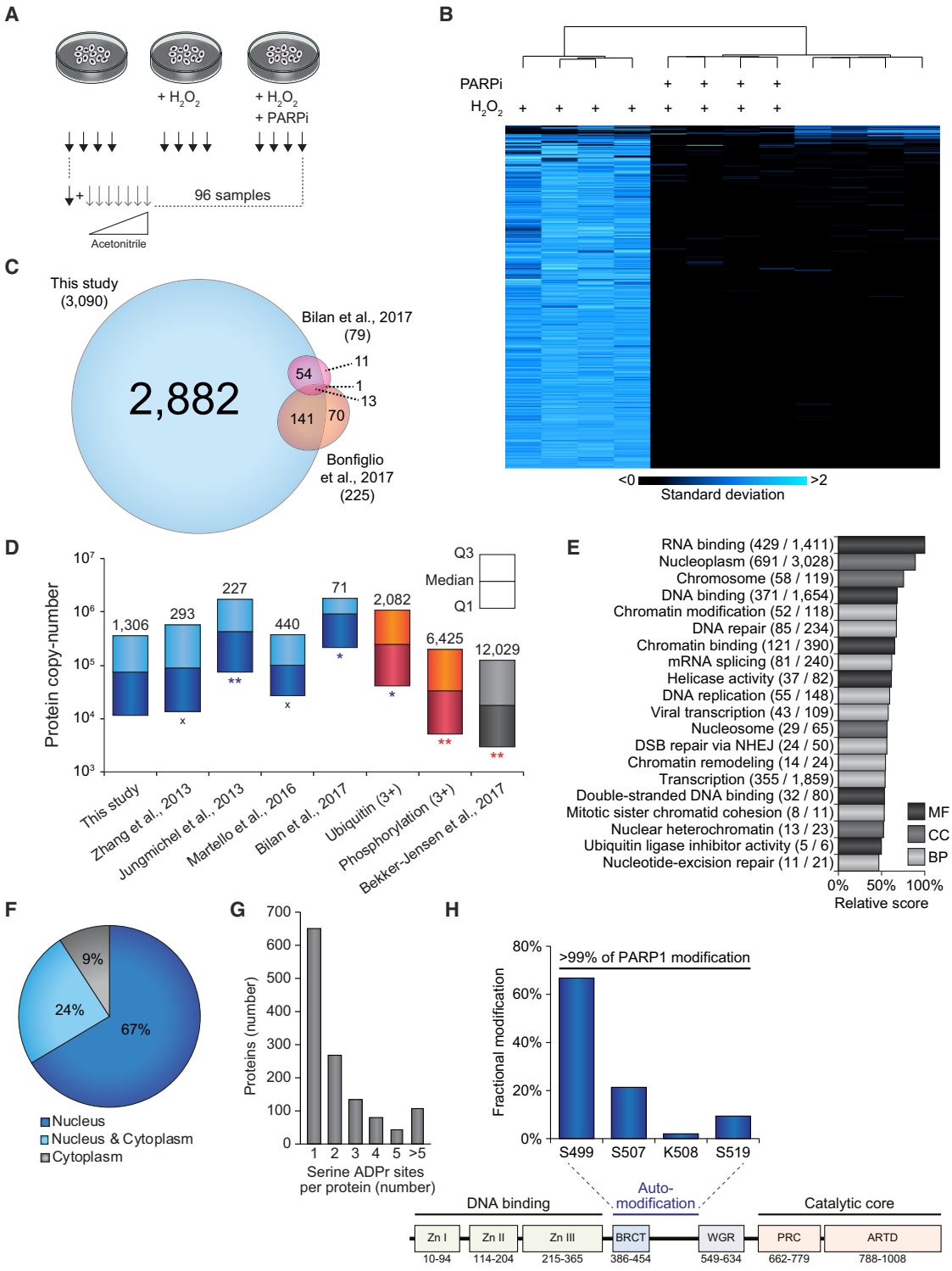


**Figure 2. Ultra-Deep Profiling of the Serine ADP-Ribosylome**

(A) Overview of the experimental design for quantitative and deep profiling of the ADP-ribosylome. The overall strategy was the same as Figure 1A, with the addition of on-StageTip high-pH fractionation of the enriched ADPr peptides (gray arrows). n = 4 cell culture replicates.

(B) Unsupervised hierarchical clustering analysis of *Z*-scored $\log_2$-transformed intensities of ADPr sites. Blue coloring indicates relative presence in a sample as compared to others.

(C) Venn diagram visualizing overlap between serine ADPr sites identified in our study compared to other ADPr proteomics studies (drawn to scale).

*(legend continued on next page)*

described high-pH (HpH) fractionation of modified peptides (Hendriks et al., 2017; Larsen et al., 2016) (Figure 2A). Although such pre-fractionation increases the overall requirements for MS acquisition time, pre-fractionation greatly improves sequencing depth of the analyzed samples (Bekker-Jensen et al., 2017). Because unrestricted analysis comes with computational limitations, we streamlined data processing by performing a semi-restricted search, allowing ADPr to reside on all amino acid residues that we detected to be ADP-ribosylated in quadruplicate in our unrestricted search (Cys, His, Arg, Ser, Thr, and Tyr), along with previously reported amino acid residues (Glu, Asp, and Lys).

Collectively, we observed a high degree of reproducibility (Figure S2A) and consistent regulation of ADPr sites in response to oxidative stress (Figure 2B). In total, we identified 3,090 serine ADPr sites with a localization probability of >90% (Table S1), hereby greatly expanding current knowledge on this emerging modification (Figure 2C) and underscoring that serine ADPr entails a broad cellular distribution. Identified serine ADPr sites mapped to 1,283 proteins (Table S2). We determined the efficiency of our purification strategy and observed a global peptide purity of 58%, with a purity of up to 95%–99% in the four most hydrophilic fractions analyzed (Table S1).

Although we mainly detected serine ADPr in response to $H_2O_2$ treatment, 358 ADPr sites were detected under control conditions and 339 ADPr sites when subjecting cells to oxidative stress in the presence of olaparib (Table S1). Thus, baseline ADPr events do occur but appear low abundant and may be technically more challenging to detect. Nonetheless, we detected >300 baseline ADPr sites, without resorting to poly (ADP-ribose) glycohydrolase (PARG) knockdown in cells to boost the numbers. Overall, ADPr on non-serine residues appeared more frequently among $H_2O_2$-unregulated ADPr sites (Table S1). We evaluated the subset of proteins exclusively modified by ADPr on non-serine residues as compared to proteins modified on at least one serine residue (Figure S2B). Intriguingly, proteins modified by ADPr on non-serine residues appeared to be more prominently localized in the cytoplasm, further solidifying that serine ADPr is a predominant nuclear modification.

To evaluate our depth of sequencing, we compared the identified ADP-ribosylome to the HeLa proteome (Bekker-Jensen et al., 2017) and other abundant PTMs, such as phosphorylation and ubiquitylation (Figure 2D; Table S3). While the deep proteome study and global knowledge on phosphorylation surpassed our study in depth of sequencing, we found that our serine ADPr analysis was on par with global knowledge of ubiquitylation (Hornbeck et al., 2012) (Figure 2D), with serine ADPr systemically occurring on less abundant proteins. When comparing our study to other recent ADPr studies (Bilan et al., 2017; Jungmichel et al., 2013; Martello et al., 2016; Zhang et al., 2013), we achieved a comparable or improved sequencing depth while detecting a considerably larger number of ADPr sites and proteins (Table S3). Overall, this emphasizes that our analysis was not biased toward abundant proteins.

Gene Ontology (GO) analysis showed a strong enrichment of biological processes associated with nuclear ARTD/PARP activities (Figure 2E; Table S4). Over 90% of identified ADPr target proteins were annotated as nuclear localized (Figure 2F), which supports previous reports that PARP1 and PARP2 are responsible for the observed increase in serine ADPr (Bonfiglio et al., 2017). This is further supported by our observation of PARP-inhibitor-dependent regulation of identified serine ADPr sites (Figure 1E). Concomitantly, PARP1 and PARP2 were themselves identified as targets of serine ADPr (Table S1), most likely induced via auto-modification (Altmeyer et al., 2009; Kim et al., 2004). When assessing the distribution of ADPr sites, we found that 51% of identified proteins harbor only one serine acceptor site, with 8% of identified proteins containing >5 modification sites (Figure 2G). Hence, the distribution of serine ADPr is relatively similar to other widespread modifications such as phosphorylation (Huttlin et al., 2010), arginine methylation (Larsen et al., 2016), and ubiquitylation (Kim et al., 2011).

Overall, we found PARP1 to be the most abundant ADPr target protein despite PARP1 not harboring the largest number of modification sites (Table 1). Next, we decided to investigate the relative contribution of individual ADPr sites as compared to the total ADPr of target proteins (Tables 1 and S1). For example, this fractional analysis demonstrated that *in vivo* >99% of ADPr on PARP1 resided within the auto-modification domain (Figure 2H), while serine ADPr within the DNA-binding region on S104, S140, and S204 constituted <1% of total ADPr on PARP1 (Table S1). Thus, our fractional analysis of ADPr events across all proteins provides another valuable dimension of biological insight.

## Sequence Properties of Serine ADPr Sites

Previous studies reported that serine ADPr sites are often preceded by basic residues (Abplanalp et al., 2017; Leidecker et al., 2016). As these studies identified a limited number of

(D) Visualization of depth of sequencing, by comparison of average protein expression levels identified across different subsets of data, as indicated. Intensity-based absolute quantification (IBAQ) copy numbers of proteins were derived from a recent deep proteome study (Bekker-Jensen et al., 2017). Blue-colored studies indicate ADPr proteomics studies. For ubiquitin and phosphorylation, only target proteins identified in three or more proteomics studies were included (PhosphoSitePlus) (Hornbeck et al., 2012). Total numbers of proteins identified are displayed above the bars. Asterisks denote significant differences between ADPr target proteins identified in this study and other datasets, with blue or red asterisks indicating whether our study achieved more or less depth, respectively. Determined by two-tailed Fisher's exact testing (*$p < 0.05$, **$p < 0.001$; x, not significant [NS]).

(E) Gene Ontology (GO) term enrichment analysis of ADPr target proteins, as compared to the human proteome (Table S4). BP, biological process; CC, cellular compartment; MF, molecular function.

(F) Pie-chart overview of the subcellular localization of serine ADPr target proteins, with localization annotations derived from Gene Ontology Cellular Component (GOCC).

(G) Distribution of serine ADPr sites per protein.

(H) Distribution of the fractional (relative to total) ADPr within the auto-modification domain of PARP1.

See also Figure S2 and Tables S1, S2, S3, and S4.

**Table 1. Fractional Modification Analysis of the ADP-Ribosylome**

| Protein | ADPr | # | # S | Primary ADPr | Fraction | Secondary ADPr | Fraction | Tertiary ADPr | Fraction | Biological Process |
|---|---|---|---|---|---|---|---|---|---|---|
| PARP1 | 1.4E+12 | 14 | 10 | S-499 | 66.8% | S-507 | 21.3% | S-519 | 9.4% | DNA repair |
| HIST1H2BC | 8.1E+11 | 14 | 7 | S-7 | 94.0% | S-15 | 5.4% | K-13 | 0.3% | nucleosome |
| HIST1H3A | 6.1E+11 | 7 | 3 | S-11 | 86.3% | S-29 | 11.1% | K-10 | 2.1% | nucleosome |
| HIST1H2BD | 2.8E+11 | 6 | 2 | S-7 | 84.5% | S-15 | 14.6% | K-13 | 0.4% | nucleosome |
| HIST2H2BF | 2.7E+11 | 5 | 2 | S-7 | 84.0% | S-15 | 15.2% | K-13 | 0.4% | nucleosome |
| HIST1H2BN | 2.4E+11 | 5 | 2 | S-7 | 81.9% | S-15 | 17.3% | K-13 | 0.4% | nucleosome |
| HIST1H1D | 2.3E+11 | 12 | 10 | S-205 | 74.2% | S-151 | 22.0% | S-56 | 1.9% | nucleosome |
| HMGA1 | 2.0E+11 | 3 | 3 | S-8 | 60.8% | S-9 | 39.2% | S-44 | 0.0% | transcription |
| HNRNPU | 1.8E+11 | 8 | 6 | S-695 | 85.1% | S-187 | 14.7% | S-690 | 0.1% | mRNA processing |
| HIST1H4A | 1.7E+11 | 2 | 1 | S-2 | 67.2% | R-4 | 32.8% | – | – | nucleosome |
| HIST1H2BL | 1.7E+11 | 5 | 2 | S-7 | 74.0% | S-15 | 24.7% | K-13 | 0.6% | nucleosome |
| HIST3H2BB | 1.7E+11 | 7 | 2 | S-7 | 73.9% | S-15 | 24.8% | K-13 | 0.6% | nucleosome |
| RFC1 | 1.6E+11 | 39 | 34 | S-302 | 31.2% | S-1126 | 22.1% | S-533 | 8.2% | DNA replication |
| DIMT1 | 1.1E+11 | 2 | 2 | S-6 | 58.6% | S-24 | 41.4% | – | – | rRNA processing |
| NPM1 | 1.1E+11 | 10 | 9 | S-195 | 39.4% | S-139 | 21.4% | S-207 | 16.5% | cell cycle |
| HIST1H1E | 8.0E+10 | 12 | 8 | S-150 | 91.2% | K-149 | 5.9% | S-102 | 1.0% | nucleosome |
| HIST3H3 | 7.9E+10 | 1 | 1 | S-29 | 100.0% | – | – | – | – | nucleosome |
| SSRP1 | 6.9E+10 | 16 | 11 | S-531 | 56.5% | S-657 | 11.2% | R-532 | 10.6% | DNA repair |
| FEN1 | 6.8E+10 | 10 | 9 | S-363 | 80.9% | S-101 | 12.0% | S-94 | 3.7% | DNA repair |
| NUCKS1 | 5.9E+10 | 4 | 4 | S-195 | 43.3% | S-39 | 31.1% | S-160 | 22.2% | DNA repair |
| DEK | 5.7E+10 | 6 | 6 | S-211 | 76.7% | S-210 | 18.3% | S-279 | 4.6% | DNA repair |
| TOP2A | 5.7E+10 | 9 | 9 | S-1449 | 43.5% | S-1452 | 30.9% | S-1423 | 17.7% | cell cycle |
| BUD23 | 4.7E+10 | 6 | 3 | S-248 | 60.6% | R-249 | 38.0% | S-240 | 1.1% | transcription |
| HIST1H1C | 4.3E+10 | 5 | 3 | S-150 | 84.1% | S-188 | 14.0% | K-152 | 0.9% | nucleosome |
| LIG3 | 4.1E+10 | 11 | 9 | S-227 | 60.0% | S-912 | 27.5% | S-876 | 5.1% | DNA repair |
| HMGB2 | 4.1E+10 | 4 | 2 | S-168 | 94.6% | K-173 | 2.8% | S-181 | 2.2% | transcription |
| NUSAP1 | 3.9E+10 | 22 | 19 | S-305 | 36.2% | H-307 | 14.6% | S-311 | 14.4% | cell cycle |
| HIST1H2BM | 3.8E+10 | 3 | 2 | S-7 | 99.1% | K-13 | 0.9% | S-15 | 0.0% | nucleosome |
| CCDC86 | 3.7E+10 | 11 | 8 | S-242 | 40.9% | R-244 | 26.7% | S-255 | 26.5% | host-virus interaction |
| HMGN2 | 3.6E+10 | 2 | 2 | S-29 | 99.6% | S-25 | 0.4% | – | – | immune response |
| CHD1L | 3.4E+10 | 11 | 10 | H-784 | 37.6% | S-780 | 19.8% | S-785 | 14.0% | DNA repair |
| RBMX | 3.0E+10 | 16 | 11 | S-157 | 27.0% | S-336 | 24.4% | S-337 | 16.5% | mRNA processing |
| KHDRBS1 | 2.9E+10 | 11 | 8 | S-18 | 65.4% | S-14 | 14.8% | R-17 | 7.8% | cell cycle |
| SUPT16H | 2.8E+10 | 12 | 10 | S-1031 | 40.1% | S-1038 | 18.8% | S-1039 | 15.4% | DNA repair |
| NOLC1 | 2.8E+10 | 12 | 11 | S-303 | 52.7% | S-669 | 30.0% | S-580 | 13.4% | cell cycle |
| LMNA | 2.7E+10 | 9 | 8 | S-12 | 89.0% | S-398 | 4.1% | S-628 | 3.1% | cell cycle |
| MKI67 | 2.3E+10 | 51 | 50 | S-621 | 35.7% | S-380 | 11.9% | S-875 | 10.1% | cell cycle |
| TMA7 | 2.3E+10 | 4 | 2 | S-61 | 95.0% | S-2 | 4.9% | T-55 | 0.1% | unknown |
| DDX21 | 2.1E+10 | 9 | 8 | S-751 | 29.5% | S-759 | 28.9% | S-731 | 19.9% | rRNA processing |
| BAZ1B | 2.0E+10 | 14 | 10 | R-455 | 42.7% | S-417 | 29.6% | S-347 | 9.9% | DNA repair |
| HMGN1 | 2.0E+10 | 4 | 4 | S-7 | 67.2% | S-25 | 30.0% | S-8 | 2.0% | DNA repair |
| GTPBP4 | 1.9E+10 | 4 | 4 | S-623 | 48.0% | S-578 | 46.4% | S-567 | 3.2% | cell cycle |
| PPHLN1 | 1.9E+10 | 9 | 6 | R-174 | 39.1% | S-110 | 31.6% | S-172 | 14.3% | transcription |
| SUB1 | 1.8E+10 | 5 | 4 | S-51 | 46.8% | S-46 | 30.5% | S-50 | 19.9% | transcription |
| NAT10 | 1.8E+10 | 2 | 2 | S-990 | 100.0% | S-984 | 0.0% | – | – | rRNA processing |
| HIST1H1A | 1.7E+10 | 3 | 3 | S-149 | 93.4% | S-124 | 4.6% | S-165 | 2.0% | nucleosome |
| EXOSC10 | 1.6E+10 | 9 | 9 | S-874 | 42.6% | S-866 | 19.7% | S-868 | 13.6% | rRNA processing |

(*Continued on next page*)

**Table 1. *Continued***

| Protein | ADPr | # | # S | Primary ADPr | Fraction | Secondary ADPr | Fraction | Tertiary ADPr | Fraction | Biological Process |
|---|---|---|---|---|---|---|---|---|---|---|
| ZNF512B | 1.5E+10 | 8 | 6 | S-18 | 63.5% | S-887 | 16.4% | S-263 | 14.2% | transcription |
| GPATCH11 | 1.4E+10 | 4 | 4 | S-84 | 49.4% | S-108 | 44.3% | S-91 | 6.3% | cell cycle |
| MITD1 | 1.4E+10 | 1 | 1 | S-4 | 100.0% | – | – | – | – | cell cycle |

An overview of the top 50 most abundantly modified ADPr target proteins. The list highlights the top three most abundant ADPr sites (Table S2), visualizing the predominant presence of serine ADPr. ADPr, total summed site intensity; #, total number of ADPr sites; #S, number of serine ADPr sites; fraction, relative contribution of this ADPr site to the total ADPr modification of the protein; biological process, Gene Ontology Biological Process.

serine ADPr sites, we decided to investigate ADPr-proximal sequence context on a wider scale (Figure 3A). We observed a strong preference for ADPr to be targeted to the lysine-serine (KS) motif, as previously described. We also observed the prevalence of a serine-glycine (SG) and, to a lesser extent, a serine-glycine-glycine (SGG) motif. Intriguingly, such sequence motifs are reminiscent of the arginine-glycine (RG) and arginine-glycine-glycine (RGG) motifs commonly targeted by arginine methylation (Thandapani et al., 2013), which our lab has previously shown to relate to the abundance of the targeted proteins (Larsen et al., 2016). Hence, we wondered if any of the observed serine ADPr motifs might reflect a similar protein abundance bias.

To investigate this, we selected subsets of ADPr target proteins harboring at least 3 modification sites, with the majority of their fractional intensity residing in either KS, or any SGG motifs, and assessed the known cellular expression levels of these proteins. We observed that proteins with a majority of ADPr residing in any SGG motifs were predominantly highly abundant proteins, suggesting the influence of protein abundance bias (Figure 3B). Intriguingly, ADPr target proteins predominantly modified on KS motifs displayed the opposite trend and thus demonstrated an anti-abundance bias. This suggests that KS motifs preferentially exist in low-abundant proteins in order to facilitate sufficient levels of ADPr in response to oxidative stress.

To further characterize serine ADPr, we performed structural-predictive analysis on all proteins modified by ADPr. This analysis determined whether serine residues in these proteins resided in disordered or globular regions and whether they were solvent exposed or buried. Overall, 59% of serine residues resided in disordered regions, whereas 75% of ADP-ribosylated serine residues resided in disordered regions (Figure 3C). The propensity of serine ADPr to target disordered regions is similar to other modifications involved in nuclear signaling, including phosphorylation (Figure 3C) (Iakoucheva et al., 2004). Hence, the shared preference for disordered regions supports previous findings where phosphorylation was observed in close proximity of ADPr sites (Gibson et al., 2016).

## Site-Specific Overlap of Serine ADPr and Phosphorylation

ADPr and phosphorylation are known to functionally interact (e.g., in the DNA damage response; Polo and Jackson, 2011), but little is currently known about the site-specific crosstalk between the two modifications (Hunter, 2007). To assess this possibility, we first compared all identified serine ADPr sites to all phosphorylation sites known to reside within ADPr target proteins (Table S4), with the phosphorylation sites derived from PhosphoSitePlus and identified in at least 3 MS screens (Hornbeck et al., 2012). Subsequently, we performed a large-scale kinase prediction on all serines co-targeted by ADPr and phosphorylation using the kinase-substrate enrichment application (KSEA) (Hornbeck et al., 2012; Linding et al., 2007). As a statistical background, we used known kinase motifs for all serine phosphorylation sites entailed in the comparison. From this analysis (Figure 3D), we found a strong enrichment for Aurora kinases A and B (AURKA and AURKB) to modulate ADPr-phospho co-targeted serines. Interestingly, AURKA and AURKB strongly associate with PARP1 activity (Monaco et al., 2005), and AURKA overexpression has been shown to result in sensitivity to the PARP inhibitor olaparib (Sourisseau et al., 2010).

To investigate this interplay in more detail, we performed quantitative phosphoproteomics analysis in HeLa cells with the same experimental conditions as used for establishing the serine ADP-ribosylome (Figure 1A). From this, we identified >27,000 class 1 phosphorylation sites (Table S5), with a high degree of reproducibility between replicates (Figures S3A and S3B). In total, ~20,000 sites could be quantified in quadruplicate, and 1,818 and 1,266 phospho sites were significantly upregulated and downregulated upon $H_2O_2$ treatment, respectively (Figure 4A; Table S5). Pretreatment of cells with PARP inhibitor did not notably modulate the phosphoproteome in response to 10 min $H_2O_2$ treatment (Figure S3C). Nonetheless, we observed a wide range of differentially regulated cellular processes for phosphoproteins that were dynamically modified in response to $H_2O2$ treatment (Figure 4B), with subtle variations in these affected processes when investigating proteins containing either downregulated or upregulated phospho sites (Figures S3D and S3E).

Interestingly, we found 483 serine ADPr sites overlapping with phosphorylation sites detected in our phosphoproteomics analysis (Figure 4C; Table S4), which represented a significantly higher degree of overlap compared to randomly expected. Thus, ADPr and phosphorylation preferentially target the same serine residues on a proteome-wide scale, with the high degree of overlap further recapitulated when comparing our serine ADP-ribosylome to literature data. Notably, the proportion of the overlap is similar to the site-specific overlap between the cross-regulatory modifications lysine acetylation and ubiquitylation (Choudhary et al., 2014).

Overlap between serine ADPr and phosphorylation significantly increased when only considering serine residues located

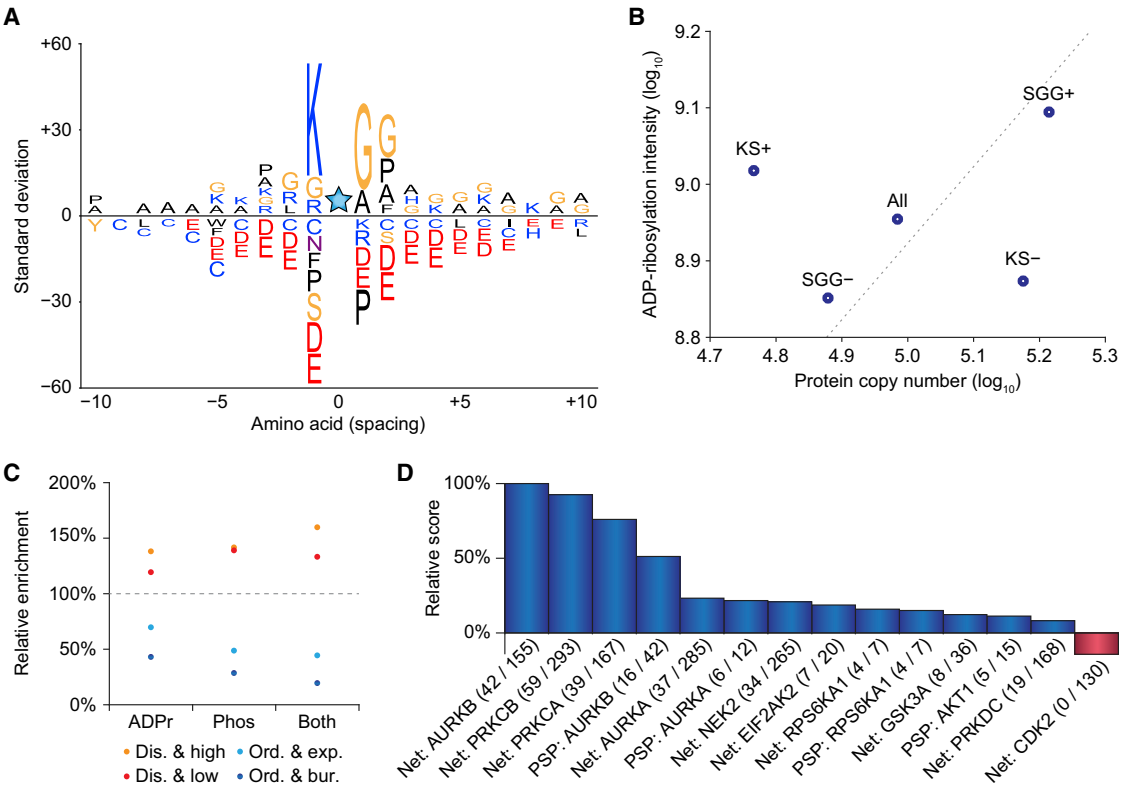


**Figure 3. Site-Specific Properties of Serine ADPr**

(A) IceLogo representation of the sequence context surrounding identified serine ADPr sites, using all serines in ADPr target proteins as a reference. Amino acids portrayed above the line are enriched, whereas amino acids below the line are depleted. Amino acid height corresponds to SD change. All changes were significant by two-tailed Student's t test with $p < 0.01$.

(B) ADPr intensity compared to protein abundance. KS and SGG indicate enriched ADPr in the corresponding motifs (+) or otherwise depleted modification (−). "All" denotes all ADPr target proteins. The dashed line represents the expected protein abundance bias.

(C) Schematic overview of structural properties of subsets of serines in human proteins targeted by ADPr as compared to structural properties of all other serines within the same proteins (Table S4). A relative presence of 100% is indicative of no change as compared to the background. Phosphorylation (Phos) sites were derived from PhosphoSitePlus and only considered if detected in 3 or more proteomics studies. "Both" corresponds to serine residues detected as ADP-ribosylated in this study and phosphorylated in PhosphoSitePlus (PSP) data. All displayed values were significant by Fisher exact testing with a Benjamini-Hochberg multiple-hypotheses corrected $p < 0.02$.

(D) Kinase enrichment analysis visualizing kinases enriched for serine residues co-targeted by ADPr and phosphorylation compared to all phosphorylated serine residues in ADPr target proteins (Table S4). Kinase predictions were extracted using the kinase-substrate enrichment application (KSEA), with information derived from NetworKIN (Net) and PSP (Hornbeck et al., 2012). All displayed values were significant by Fisher exact testing with a Benjamini-Hochberg multiple-hypotheses corrected $p < 0.02$.

See also Table S4.

outside of the canonical phosphorylation serine-proline (SP) motif (Figure 4C). Similarly, when considering ADPr-phospho crosstalk outside of the ADPr-preferred KS motifs, we again observed a significantly higher degree of overlap. To further this, we evaluated the relative preferences of ADPr and phosphorylation for targeting KS motifs (Figure 4D) and found a strong preference for ADPr to target these motifs, contrary to phosphorylation. When considering SP motifs (Figure 4E), we confirmed the preference of phosphorylation to be targeted to these motifs but moreover a highly significant propensity for ADPr to entirely avert targeting SP motifs. SP-driven phosphorylation sites typically constitute the majority of identified phosphorylation sites in standard proteomics experiments (Huttlin et al., 2010), and thus the aversion of serine ADPr to SP motifs seemed quite remarkable. With cyclin-dependent kinases (CDKs) typically responsible for catalyzing phosphorylation of SP motifs (Amanchy et al., 2007), site-specific regulation of ADPr may functionally not relate to biological processes involving CDK activity. No kinase has been reported to catalyze phosphorylation in KS motifs, and although serine ADPr preferentially localized to KS motifs (Figures 3A and 4D), the overlapping modification sites were more frequently observed outside of KS motifs (Figure 4C).

To assess the effect of ADPr on phosphorylation and the potential involvement of kinases in a more direct manner, we analyzed the propensity of ADPr, phosphorylation, or both to modify serines residing within all known kinase motifs in the co-targeted proteins (Figure 4F; Tables S4 and S5). We observed

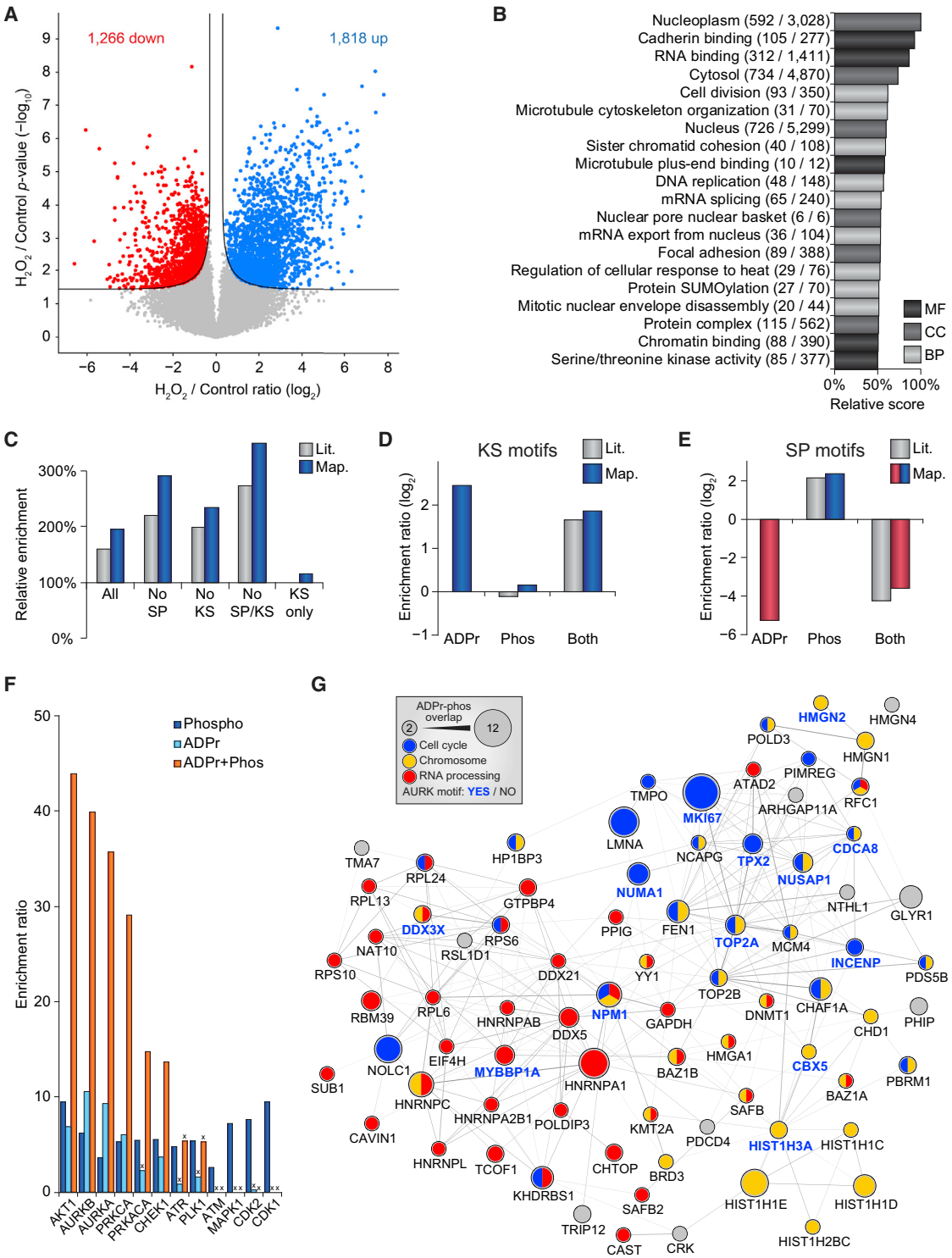


**Figure 4. Co-targeting of ADPr and Phospho to Serines and Kinase Motifs**

(A) Volcano plot analysis to visualize phosphorylation dynamics in response to $H_2O_2$ treatment. Red, silver, and blue dots indicate downregulated, non-regulated, and upregulated phospho sites, respectively. n = 4 cell culture replicates, $q$-value < 0.05 for significance; permutation-based false discovery rate (FDR) calculated at an s0 of 0.1.

*(legend continued on next page)*

several kinase motifs to be strongly enriched for co-targeting by both phosphorylation and serine ADPr, with RAC-alpha serine/threonine-protein kinase (AKT1), AURKA and AURKB, and protein kinase C (PRKCA and PRKACA) being among the top hits. Likewise, we noted a PARP-dependent effect on the directional regulation of phosphorylation sites preferentially modulated by the AKT1, AURKB, PRKCA, and PRKACA kinases (Figure S4A).

Interestingly, among the identified serine ADPr sites, we observed a stronger enrichment for modification of AURKA/B kinase motifs, as compared to the corresponding phosphorylation sites (Figure 4F). Using immunoblot analysis, we confirmed that the activity of AURKA/B is temporally regulated in a PARP-dependent manner (Figure S4B). Similarly, the phosphorylation status of known AURKB substrates histone H3 (Ser10) and transforming acidic coiled-coil-containing protein 3 (TACC3, Ser558) were PARP dependent (Figures S4D and S4E). Considering that AURKA, AURKB, and histone H3 Ser10 were ADP ribosylated in our dataset, this supports the regulatory interplay between the modifications.

In spite of overlapping sites between serine ADPr and phosphorylation infrequently occurring in SP motifs, the proteins harboring co-targeted modification sites were observed to be functionally interconnected and moreover globally relate to the cell cycle (Figure 4G). This suggested that while phosphorylation sites catalyzed by CDKs might not participate in direct crosstalk with serine ADPr, the site-specific crosstalk between the modifications could still play a functional role in cell cycle regulation (Adolph, 1985).

Collectively, our data suggest alignment in the directionality of ADPr and phosphorylation in the early response to oxidative damage and that shared targeting of same serine residues by PARP enzymes and the Aurora kinases may entail a hitherto uncharacterized layer in cellular signaling.

## DISCUSSION

Here, we describe proteome-wide identification of serine ADPr sites in human cells and provide quantitative insights into serine ADPr dynamics upon oxidative stress. In total, we report identification of 3,090 serine ADPr sites, providing an in-depth compendium of the human serine ADP-ribosylome. The proteins targeted by serine ADPr prominently localize to the nucleus, which together with our quantitative analyses demonstrate that serine ADPr is a major nuclear responder to oxidative stress. Many regulatory systems exist in human cells, and serine ADPr appears to be intricately involved, with the modification targeting ubiquitin ligases, protein kinases, methyltransferases, RNA-interacting proteins, and numerous other enzymes involved in cellular signaling events. Our data furthermore highlight that the ADPr stimulus is distributed to transcriptional regulators and co-regulators during oxidative stress.

Notably, the distribution of ADP-ribosylated amino acids observed in our dataset differs from previous reports describing glutamic and aspartic acid as targets of ADPr (Gibson et al., 2016; Zhang et al., 2013; Zhen et al., 2017). These studies utilized an analytical strategy directed toward ADPr on acidic residues only and were thus incapable of identifying serine ADPr. Although our strategy does not suffer from this limitation (Figure 1; Data S1), our dataset does not entail a similar extent of ADPr of glutamic and aspartic acids. Considering that the Af1521 domain does not exhibit any hydrolase activity during our experimental conditions (Jungmichel et al., 2013; Martello et al., 2016), our data suggest that serine ADPr is more abundantly present in human cells than ADPr of glutamic and aspartic acids. Furthering this, most proteins modified on non-serine residues in our dataset were also modified on one or more serine residues (Table S2), which could explain why targeted strategies are required for the investigation of ADPr on acidic residues (Zhang et al., 2013). The cellular abundance difference is further supported by a recent observation using complementary approaches, where serine ADPr was reported to constitute a major target during DNA damage, and where co-factor HPF1 was shown to direct the catalytic amino acid preference of PARP enzymes to serine residues (Bonfiglio et al., 2017).

Whether the extent of the serine ADP-ribosylome reported in the current study primarily depends upon HPF1 (Gibbs-Seymour et al., 2016) remains to be determined. However, treating cells with olaparib abrogated the cellular induction of serine ADPr in response to $H_2O_2$, suggesting that serine ADPr represents the

(B) GO term enrichment analysis of dynamically phosphorylated proteins upon $H_2O_2$ treatment as compared to the human proteome (Table S4). BP, biological processes; CC, cellular compartments, MF, molecular functions. All displayed values were significant by Fisher exact testing with a Benjamini-Hochberg multiple-hypotheses corrected $p < 0.02$.

(C) Relative overlap between subsets of serine residues modified by ADPr and phosphorylation. A relative overlap of 100% is indicative of no change as compared to the background. All displayed values were significant by Fisher exact testing with a Benjamini Hochberg multiple hypotheses corrected $p < 0.02$. Lit., phospho sites derived from PSP, detected in 3 or more proteomics studies; Map., phospho sites derived from our phosphoproteomics experiments.

(D) Propensity of serines targeted by ADPr, phosphorylation, or both, to reside in KS motifs. Lit., phospho sites derived from PSP and only considered if detected in 3 or more proteomics studies; Map., phospho sites mapped in this study.

(E) As in (D), but for SP motifs.

(F) Kinase enrichment analysis based on our experimental data, visualizing the propensity of serine residues to reside in known kinase motifs when they are modified by phosphorylation, ADPr, or both PTMs. As a background, all serine residues in ADPr target proteins were considered, and all known kinase motifs were extracted from PSP and aligned to these serines (754 kinase motifs and 89,012 serines; Table S4). All displayed values were significant by Fisher exact testing with a Benjamini Hochberg multiple hypotheses corrected $p < 0.05$, unless indicated with an "x." Statistical information is further detailed in Table S4.

(G) Search Tool for the Retrieval of Interacting Genes/Proteins (STRING) network visualizing functional interactions between proteins with at least two serine residues co-targeted by ADPr and phosphorylation based on our experimental data. Default STRING clustering confidence was used ($p > 0.4$), and disconnected proteins were omitted from the network. Nodes corresponding to proteins were annotated with visual properties, as highlighted in the figure legend. ADPr-phos overlap, number of co-targeted serine residues; AURK motif, at least one co-targeted serine residue is modulated by AURKA or AURKB.

See also Figures S3 and S4 and Tables S4 and S5.

primary biological mode of action. Olaparib is used in the clinic as a therapeutic agent for treatment of ovarian and breast cancer, and our dataset detailing the molecular targets of the inhibitor may consequently aid in a better understanding of the molecular mechanism related to clinical resistance of PARP inhibitor treatment.

Notably, the extent of serine ADPr sites reported herein differs from previous observations (Martello et al., 2016), as previous mass spectrometric and bioinformatics approaches were not configured to facilitate detection of the recently reported serine ADPr. Our current strategy does not suffer from such limitations and facilitates purification and detection of any amino acid residue being modified by ADPr. However, a limitation of our approach is that it cannot address whether identified ADPr sites were initially MAR or PAR, as this information is lost during PARG treatment. However, considering serine ADPr is primarily catalyzed by PARP1, we assume that the majority of identified sites represent PARylation.

To demonstrate the potential of our resource to derive biological insights that are not easily obtainable through low-throughput strategies, we determined the fractional contribution of all serine ADPr sites to the total ADPr abundance of individual target proteins. In turn, this provides valuable quantitative insights into the site-specific levels of ADPr and constitutes a valuable resource for generation of separation-of-function mutations in proteins targeted by serine ADPr.

Full-scale structural-predictive analysis demonstrated that serine ADPr preferentially targeted disordered regions in target proteins. Thus, the structural preference of the PARP1/2 enzymes is similar to those catalyzing other widespread modifications, including phosphorylation kinases and the SUMO enzymatic machinery. As cancer-associated and signaling proteins tend to have a higher proportion of residues in disordered regions compared to other proteins (Iakoucheva et al., 2002), the observed preference of serine ADPr could indicate a more prevalent involvement in cellular signaling than currently anticipated.

Our data reveal evidence of a shared targeting preference between serine ADPr and phosphorylation, with identified serine ADPr sites significantly overlapping with serine phosphorylation sites, suggesting site-specific regulatory interplay between the two modifications. Such interplay has previously been observed on histones, where the overall phosphorylation status of histones was reduced upon ADPr (Tanigawa et al., 1983). Intriguingly, we observed several ADPr sites to overlap with known histone phosphorylation sites (Table S1), which may account for the observed regulatory phenotype. However, it remains to be investigated whether the observed overlap codifies a negative crosstalk, where one modification outcompetes the other, or a positive crosstalk, where one modification temporarily precedes the other (Hunter, 2007).

Phosphoproteomics and kinase-prediction analyses revealed a strong propensity for ADPr to target serine residues that are modulated in phosphorylation status through the action of AURKA/B. Moreover, we find both AURKA/B to be modified by serine ADPr, and ADPr was previously shown to affect AURKB kinase activity (Monaco et al., 2005). With overexpression of AURKA reported to lead to an enhanced sensitivity to PARP inhibitors (Sourisseau et al., 2010), our observations provide insight into an emerging and site-specific interplay between serine ADPr catalyzed by PARP and phosphorylation catalyzed by AURKA/B. For example, among proteins targeted by modifications on same serine residues, we noticed that breast cancer type 1 susceptibility protein (BRCA1) is modified with ADPr on serine 308 (Table S1). The same serine residue constitutes a known phosphorylation target of AURKA, which upon phosphorylation of BRCA1 leads to increased microtubule assembly rates and chromosome missegregation (Ertych et al., 2016). Because BRCA-defective tumors are particularly sensitive to PARP inhibitors following the concept of synthetic lethality and loss of BRCA1 or BRCA2 function results in sensitivity to the inhibition of PARP (Helleday, 2011), site-specific regulation of phosphorylation and serine ADPr on BRCA1 could constitute a regulatory layer within the synthetic lethality of PARP inhibitors (Helleday, 2011). Along these lines, the PARP inhibitor olaparib has been described as a strong inducer of chromosome missegregation in human cells (Colicchia et al., 2017; Lee et al., 2016). While this underscores the complex interplay between various modifications and the proteins they target, it also displays the necessity for systems-wide proteomics analyses to gain valuable biological insight into the regulatory scope of currently obscure modifications. Collectively, the presented human serine ADP-ribosylome provides a missing piece in the global and integrative view of cellular physiology and comprises a vast biological resource.

## STAR★METHODS

Detailed methods are provided in the online version of this paper and include the following:

- KEY RESOURCES TABLE
- CONTACT FOR REAGENT AND RESOURCE SHARING
- EXPERIMENTAL MODEL AND SUBJECT DETAILS
  - Cell lines
  - Bacteria
- METHOD DETAILS
  - Cell treatment
  - Cell lysis and sample preparation
  - Purification of GST-tagged Af1521 macrodomain
  - Enrichment of ADP-ribosylated peptides
  - Enrichment of phosphorylated peptides
  - Fractionation of peptides by StageTip
  - Mass spectrometric analysis
  - Data analysis
  - Validation of ADPr on CHTY residues
  - Western blot analysis
- QUANTIFICATION AND STATISTICAL ANALYSIS
- DATA AND SOFTWARE AVAILABILITY

## SUPPLEMENTAL INFORMATION

Supplemental Information includes four figures, five tables, and one data file and can be found with this article online at https://doi.org/10.1016/j.celrep.2018.07.083.

## ACKNOWLEDGMENTS

The work carried out in this study was in part supported by the Novo Nordisk Foundation Center for Protein Research, the Novo Nordisk Foundation (grant agreements NNF14CC0001 and NNF13OC0006477), and the Danish Council for Independent Research (grant agreements DFF 4002-00051 and DFF 4183-00322A. I.A.H. is supported by the European Molecular Biology Organization (grant agreement ALTF 503-2016). We would like to acknowledge the lab of Michael O. Hottiger for the expression and purification of recombinant human PARG (University of Zurich), and we thank members of the NNF-CPR Mass Spectrometry Platform for instrument support and technical assistance.

## AUTHOR CONTRIBUTIONS

S.C.L. and I.A.H. prepared all samples, performed all experiments, and measured all samples on MS. I.A.H., S.C.L., and M.L.N. processed all MS raw data. I.A.H. and S.C.L. optimized MS methodology and performed all bioinformatics and statistical analyses. D.L. and L.J.J. performed structural predictions. M.L.N. supervised the project. M.L.N., I.A.H., and S.C.L. conceived the project and wrote the manuscript.

## DECLARATION OF INTERESTS

The authors declare no competing interests.

Received: March 15, 2018
Revised: May 31, 2018
Accepted: July 25, 2018
Published: August 28, 2018

## REFERENCES

Abplanalp, J., Leutert, M., Frugier, E., Nowak, K., Feurer, R., Kato, J., Kistemaker, H.V.A., Filippov, D.V., Moss, J., Caflisch, A., and Hottiger, M.O. (2017). Proteomic analyses identify ARH3 as a serine mono-ADP-ribosylhydrolase. Nat. Commun. *8*, 2055.

Adolph, K.W. (1985). Cell cycle variations in ADP-ribosylation of HeLa nuclear proteins. Arch. Biochem. Biophys. *243*, 427–438.

Altmeyer, M., Messner, S., Hassa, P.O., Fey, M., and Hottiger, M.O. (2009). Molecular mechanism of poly(ADP-ribosyl)ation by PARP1 and identification of lysine residues as ADP-ribose acceptor sites. Nucleic Acids Res. *37*, 3723–3738.

Amanchy, R., Periaswamy, B., Mathivanan, S., Reddy, R., Tattikota, S.G., and Pandey, A. (2007). A curated compendium of phosphorylation motifs. Nat. Biotechnol. *25*, 285–286.

Bekker-Jensen, D.B., Kelstrup, C.D., Batth, T.S., Larsen, S.C., Haldrup, C., Bramsen, J.B., Sørensen, K.D., Høyer, S., Ørntoft, T.F., Andersen, C.L., et al. (2017). An optimized shotgun strategy for the rapid generation of comprehensive human proteomes. Cell Syst. *4*, 587–599.e4.

Bilan, V., Leutert, M., Nanni, P., Panse, C., and Hottiger, M.O. (2017). Combining higher-energy collision dissociation and electron-transfer/higher-energy collision dissociation fragmentation in a product-dependent manner confidently assigns proteomewide ADP-ribose acceptor sites. Anal. Chem. *89*, 1523–1530.

Bonfiglio, J.J., Fontana, P., Zhang, Q., Colby, T., Gibbs-Seymour, I., Atanassov, I., Bartlett, E., Zaja, R., Ahel, I., and Matic, I. (2017). Serine ADP-ribosylation depends on HPF1. Mol. Cell *65*, 932–940.e6.

Casado, P., Rodriguez-Prados, J.C., Cosulich, S.C., Guichard, S., Vanhaesebroeck, B., Joel, S., and Cutillas, P.R. (2013). Kinase-substrate enrichment analysis provides insights into the heterogeneity of signaling pathway activation in leukemia cells. Sci. Signal. *6*, rs6.

Choudhary, C., Weinert, B.T., Nishida, Y., Verdin, E., and Mann, M. (2014). The growing landscape of lysine acetylation links metabolism and cell signalling. Nat. Rev. Mol. Cell Biol. *15*, 536–550.

Colaert, N., Helsens, K., Martens, L., Vandekerckhove, J., and Gevaert, K. (2009). Improved visualization of protein consensus sequences by iceLogo. Nat. Methods *6*, 786–787.

Colicchia, V., Petroni, M., Guarguaglini, G., Sardina, F., Sahún-Roncero, M., Carbonari, M., Ricci, B., Heil, C., Capalbo, C., Belardinilli, F., et al. (2017). PARP inhibitors enhance replication stress and cause mitotic catastrophe in MYCN-dependent neuroblastoma. Oncogene *36*, 4682–4691.

Coon, J.J., Ueberheide, B., Syka, J.E., Dryhurst, D.D., Ausio, J., Shabanowitz, J., and Hunt, D.F. (2005). Protein identification using sequential ion/ion reactions and tandem mass spectrometry. Proc. Natl. Acad. Sci. USA *102*, 9463–9468.

Cox, J., Hein, M.Y., Luber, C.A., Paron, I., Nagaraj, N., and Mann, M. (2014). Accurate proteome-wide label-free quantification by delayed normalization and maximal peptide ratio extraction, termed MaxLFQ. Mol. Cell. Proteomics *13*, 2513–2526.

Ertych, N., Stolz, A., Valerius, O., Braus, G.H., and Bastians, H. (2016). CHK2-BRCA1 tumor-suppressor axis restrains oncogenic Aurora-A kinase to ensure proper mitotic microtubule assembly. Proc. Natl. Acad. Sci. USA *113*, 1817–1822.

Fontana, P., Bonfiglio, J.J., Palazzo, L., Bartlett, E., Matic, I., and Ahel, I. (2017). Serine ADP-ribosylation reversal by the hydrolase ARH3. eLife *6*, 6.

Gibbs-Seymour, I., Fontana, P., Rack, J.G.M., and Ahel, I. (2016). HPF1/C4orf27 is a PARP-1-interacting protein that regulates PARP-1 ADP-ribosylation activity. Mol. Cell *62*, 432–442.

Gibson, B.A., and Kraus, W.L. (2012). New insights into the molecular and cellular functions of poly(ADP-ribose) and PARPs. Nat. Rev. Mol. Cell Biol. *13*, 411–424.

Gibson, B.A., Zhang, Y., Jiang, H., Hussey, K.M., Shrimp, J.H., Lin, H., Schwede, F., Yu, Y., and Kraus, W.L. (2016). Chemical genetic discovery of PARP targets reveals a role for PARP-1 in transcription elongation. Science *353*, 45–50.

Gupte, R., Liu, Z., and Kraus, W.L. (2017). PARPs and ADP-ribosylation: recent advances linking molecular functions to biological outcomes. Genes Dev. *31*, 101–126.

Helleday, T. (2011). The underlying mechanism for the PARP and BRCA synthetic lethality: clearing up the misunderstandings. Mol. Oncol. *5*, 387–393.

Hendriks, I.A., Lyon, D., Young, C., Jensen, L.J., Vertegaal, A.C., and Nielsen, M.L. (2017). Site-specific mapping of the human SUMO proteome reveals co-modification with phosphorylation. Nat. Struct. Mol. Biol. *24*, 325–336.

Hornbeck, P.V., Kornhauser, J.M., Tkachev, S., Zhang, B., Skrzypek, E., Murray, B., Latham, V., and Sullivan, M. (2012). PhosphoSitePlus: a comprehensive resource for investigating the structure and function of experimentally determined post-translational modifications in man and mouse. Nucleic Acids Res. *40*, D261–D270.

Hottiger, M.O. (2015). Nuclear ADP-Ribosylation and Its Role in Chromatin Plasticity, Cell Differentiation, and Epigenetics. Annu. Rev. Biochem. *84*, 227–263.

Hottiger, M.O., Hassa, P.O., Lüscher, B., Schüler, H., and Koch-Nolte, F. (2010). Toward a unified nomenclature for mammalian ADP-ribosyltransferases. Trends Biochem. Sci. *35*, 208–219.

Hunter, T. (2007). The age of crosstalk: phosphorylation, ubiquitination, and beyond. Mol. Cell *28*, 730–738.

Huttlin, E.L., Jedrychowski, M.P., Elias, J.E., Goswami, T., Rad, R., Beausoleil, S.A., Villén, J., Haas, W., Sowa, M.E., and Gygi, S.P. (2010). A tissue-specific atlas of mouse protein phosphorylation and expression. Cell *143*, 1174–1189.

Iakoucheva, L.M., Brown, C.J., Lawson, J.D., Obradović, Z., and Dunker, A.K. (2002). Intrinsic disorder in cell-signaling and cancer-associated proteins. J. Mol. Biol. *323*, 573–584.

Iakoucheva, L.M., Radivojac, P., Brown, C.J., O'Connor, T.R., Sikes, J.G., Obradovic, Z., and Dunker, A.K. (2004). The importance of intrinsic disorder for protein phosphorylation. Nucleic Acids Res. *32*, 1037–1049.

Jungmichel, S., Rosenthal, F., Altmeyer, M., Lukas, J., Hottiger, M.O., and Nielsen, M.L. (2013). Proteome-wide identification of poly(ADP-Ribosyl)ation targets in different genotoxic stress responses. Mol. Cell *52*, 272–285.

Kim, M.Y., Mauro, S., Gévry, N., Lis, J.T., and Kraus, W.L. (2004). NAD+-dependent modulation of chromatin structure and transcription by nucleosome binding properties of PARP-1. Cell *119*, 803–814.

Kim, W., Bennett, E.J., Huttlin, E.L., Guo, A., Li, J., Possemato, A., Sowa, M.E., Rad, R., Rush, J., Comb, M.J., et al. (2011). Systematic and quantitative assessment of the ubiquitin-modified proteome. Mol. Cell *44*, 325–340.

Larsen, S.C., Sylvestersen, K.B., Mund, A., Lyon, D., Mullari, M., Madsen, M.V., Daniel, J.A., Jensen, L.J., and Nielsen, M.L. (2016). Proteome-wide analysis of arginine monomethylation reveals widespread occurrence in human cells. Sci. Signal. *9*, rs9.

Lee, H.S., Lee, N.C., Kouprina, N., Kim, J.H., Kagansky, A., Bates, S., Trepel, J.B., Pommier, Y., Sackett, D., and Larionov, V. (2016). Effects of anticancer drugs on chromosome instability and new clinical implications for tumor-suppressing therapies. Cancer Res. *76*, 902–911.

Leidecker, O., Bonfiglio, J.J., Colby, T., Zhang, Q., Atanassov, I., Zaja, R., Palazzo, L., Stockum, A., Ahel, I., and Matic, I. (2016). Serine is a new target residue for endogenous ADP-ribosylation on histones. Nat. Chem. Biol. *12*, 998–1000.

Leung, A.K.L. (2017). PARPs. Curr. Biol. *27*, R1256–R1258.

Linding, R., Jensen, L.J., Ostheimer, G.J., van Vugt, M.A., Jørgensen, C., Miron, I.M., Diella, F., Colwill, K., Taylor, L., Elder, K., et al. (2007). Systematic discovery of in vivo phosphorylation networks. Cell *129*, 1415–1426.

Lord, C.J., and Ashworth, A. (2017). PARP inhibitors: synthetic lethality in the clinic. Science *355*, 1152–1158.

Martello, R., Leutert, M., Jungmichel, S., Bilan, V., Larsen, S.C., Young, C., Hottiger, M.O., and Nielsen, M.L. (2016). Proteome-wide identification of the endogenous ADP-ribosylome of mammalian cells and tissue. Nat. Commun. *7*, 12917.

Molina, H., Horn, D.M., Tang, N., Mathivanan, S., and Pandey, A. (2007). Global proteomic profiling of phosphopeptides using electron transfer dissociation tandem mass spectrometry. Proc. Natl. Acad. Sci. USA *104*, 2199–2204.

Monaco, L., Kolthur-Seetharam, U., Loury, R., Murcia, J.M., de Murcia, G., and Sassone-Corsi, P. (2005). Inhibition of Aurora-B kinase activity by poly(ADP-ribosyl)ation in response to DNA damage. Proc. Natl. Acad. Sci. USA *102*, 14244–14248.

Palazzo, L., Leidecker, O., Prokhorova, E., Dauben, H., Matic, I., and Ahel, I. (2018). Serine is the major residue for ADP-ribosylation upon DNA damage. eLife *7*, e34334.

Polo, S.E., and Jackson, S.P. (2011). Dynamics of DNA damage response proteins at DNA breaks: a focus on protein modifications. Genes Dev. *25*, 409–433.

Pommier, Y., O'Connor, M.J., and de Bono, J. (2016). Laying a trap to kill cancer cells: PARP inhibitors and their mechanisms of action. Sci. Transl. Med. *8*, 362ps17.

Rappsilber, J., Ishihama, Y., and Mann, M. (2003). Stop and go extraction tips for matrix-assisted laser desorption/ionization, nanoelectrospray, and LC/MS sample pretreatment in proteomics. Anal. Chem. *75*, 663–670.

Rose, C.M., Rush, M.J., Riley, N.M., Merrill, A.E., Kwiecien, N.W., Holden, D.D., Mullen, C., Westphall, M.S., and Coon, J.J. (2015). A calibration routine for efficient ETD in large-scale proteomics. J Am Soc Mass Spectrom. *26*, 1848–1857.

Rouleau, M., Patel, A., Hendzel, M.J., Kaufmann, S.H., and Poirier, G.G. (2010). PARP inhibition: PARP1 and beyond. Nat. Rev. Cancer *10*, 293–301.

Schreiber, V., Dantzer, F., Ame, J.C., and de Murcia, G. (2006). Poly(ADP-ribose): novel functions for an old molecule. Nat. Rev. Mol. Cell Biol. *7*, 517–528.

Seman, M., Adriouch, S., Haag, F., and Koch-Nolte, F. (2004). Ecto-ADP-ribosyltransferases (ARTs): emerging actors in cell communication and signaling. Curr. Med. Chem. *11*, 857–872.

Senko, M.W., Remes, P.M., Canterbury, J.D., Mathur, R., Song, Q., Eliuk, S.M., Mullen, C., Earley, L., Hardman, M., Blethrow, J.D., et al. (2013). Novel parallelized quadrupole/linear ion trap/Orbitrap tribrid mass spectrometer improving proteome coverage and peptide identification rates. Anal. Chem. *85*, 11710–11714.

Shannon, P., Markiel, A., Ozier, O., Baliga, N.S., Wang, J.T., Ramage, D., Amin, N., Schwikowski, B., and Ideker, T. (2003). Cytoscape: a software environment for integrated models of biomolecular interaction networks. Genome Res. *13*, 2498–2504.

Sourisseau, T., Maniotis, D., McCarthy, A., Tang, C., Lord, C.J., Ashworth, A., and Linardopoulos, S. (2010). Aurora-A expressing tumour cells are deficient for homology-directed DNA double strand-break repair and sensitive to PARP inhibition. EMBO Mol. Med. *2*, 130–142.

Syka, J.E., Coon, J.J., Schroeder, M.J., Shabanowitz, J., and Hunt, D.F. (2004). Peptide and protein sequence analysis by electron transfer dissociation mass spectrometry. Proc. Natl. Acad. Sci. USA *101*, 9528–9533.

Szklarczyk, D., Franceschini, A., Wyder, S., Forslund, K., Heller, D., Huerta-Cepas, J., Simonovic, M., Roth, A., Santos, A., Tsafou, K.P., et al. (2015). STRING v10: protein-protein interaction networks, integrated over the tree of life. Nucleic Acids Res. *43*, D447–D452.

Tanigawa, Y., Tsuchiya, M., Imai, Y., and Shimoyama, M. (1983). Mono (ADP-ribosyl)ation of hen liver nuclear proteins suppresses phosphorylation. Biochem. Biophys. Res. Commun. *113*, 135–141.

Thandapani, P., O'Connor, T.R., Bailey, T.L., and Richard, S. (2013). Defining the RGG/RG motif. Mol. Cell *50*, 613–623.

Tyanova, S., Temu, T., Sinitcyn, P., Carlson, A., Hein, M.Y., Geiger, T., Mann, M., and Cox, J. (2016). The Perseus computational platform for comprehensive analysis of (prote)omics data. Nat. Methods *13*, 731–740.

Ueda, K., and Hayaishi, O. (1985). ADP-ribosylation. Annu. Rev. Biochem. *54*, 73–100.

Vivelo, C.A., Wat, R., Agrawal, C., Tee, H.Y., and Leung, A.K. (2017). ADPriboDB: the database of ADP-ribosylated proteins. Nucleic Acids Res. *45* (*D1*), D204–D209.

Vizcaíno, J.A., Côté, R.G., Csordas, A., Dianes, J.A., Fabregat, A., Foster, J.M., Griss, J., Alpi, E., Birim, M., Contell, J., et al. (2013). The PRoteomics IDEntifications (PRIDE) database and associated tools: status in 2013. Nucleic Acids Res. *41*, D1063–D1069.

Wahlberg, E., Karlberg, T., Kouznetsova, E., Markova, N., Macchiarulo, A., Thorsell, A.G., Pol, E., Frostell, Å., Ekblad, T., Öncü, D., et al. (2012). Family-wide chemical profiling and structural analysis of PARP and tankyrase inhibitors. Nat. Biotechnol. *30*, 283–288.

Zee, B.M., and Garcia, B.A. (2010). Electron transfer dissociation facilitates sequencing of adenosine diphosphate-ribosylated peptides. Anal. Chem. *82*, 28–31.

Zhang, Y., Wang, J., Ding, M., and Yu, Y. (2013). Site-specific characterization of the Asp- and Glu-ADP-ribosylated proteome. Nat. Methods *10*, 981–984.

Zhen, Y., Zhang, Y., and Yu, Y. (2017). A cell-line-specific atlas of PARP-mediated protein Asp/Glu-ADP-ribosylation in breast cancer. Cell Rep. *21*, 2326–2337.

Zubarev, R.A., Kelleher, N.L., and McLafferty, F.W. (1998). Electron capture dissociation of multiply charged protein cations. A nonergodic process. J. Am. Chem. Soc. *120*, 3265–3266.

# STAR★METHODS

## KEY RESOURCES TABLE

| REAGENT or RESOURCE | SOURCE | IDENTIFIER |
|---|---|---|
| Antibodies | | |
| Phospho-Aurora A (Thr288)/Aurora B (Thr232)/Aurora C (Thr198) rabbit mAb | Cell Signaling Technology | Cat#2914T; RRID: AB_2061631 |
| Phospho-Histone H3 (Ser10) rabbit mAb | Cell Signaling Technology | Cat#3377; RRID: AB_1549592 |
| Phospho-TACC3 (Ser558) rabbit mAb | Cell Signaling Technology | Cat#8842; RRID: AB_10889083 |
| Goat-anti-rabbit | Jackson Immunoresearch | Cat#111-036-045; RRID: AB_2337943 |
| Bacterial and Virus Strains | | |
| BL21(DE3) | New England BioLabs | Cat#C2527I |
| Chemicals, Peptides, and Recombinant Proteins | | |
| Hydrogen peroxide ($H_2O_2$) | Sigma Aldrich | Cat#H1009 |
| Olaparib (AZD2281, KU-0059436) | Selleckchem | Cat#S1060 |
| Lysyl Endopeptidase (Lys-C) | Wako Chemicals | Cat#129-02541 |
| Trypsin, Proteomics Grade | Sigma Aldrich | Cat#T6567 |
| Recombinant PARG enzyme | Prof. Dr. Michael O. Hottiger | N/A |
| Recombinant GST-tagged Af1521 | Martello et al., 2016 | N/A |
| Titanium dioxide ($TiO_2$) | GL Sciences | Cat#GL-5020-75000 |
| Deposited Data | | |
| Raw and analyzed ADP-ribosylation MS data | This paper | ProteomeXchange: PXD009208 |
| Raw and analyzed phosphorylation MS data | This paper | ProteomeXchange: PXD009931 |
| Experimental Models: Cell Lines | | |
| HeLa | ATCC | CCL-2 |

## CONTACT FOR REAGENT AND RESOURCE SHARING

Further information and requests for resources and reagents should be directed to and will be fulfilled by the Lead Contact, Michael Lund Nielsen (michael.lund.nielsen@cpr.ku.dk).

## EXPERIMENTAL MODEL AND SUBJECT DETAILS

### Cell lines

HeLa cells (CCL-2, female) were acquired from the American Type Culture Collection, and cultured in Dulbecco's modified Eagle's medium (Invitrogen) supplemented with 10% fetal bovine serum and penicillin/streptomycin (100 U/mL; GIBCO) at 37°C and 5% $CO_2$. Cells were not routinely authenticated. Cells were routinely tested for mycoplasma contamination.

### Bacteria

BL21(DE3) Competent *E. coli* were acquired from New England BioLabs. Details regarding culture conditions are outlined in the method details.

## METHOD DETAILS

### Cell treatment

In order to study ADP-ribosylation in the context of the DNA damage response, ~75 million HeLa cells were cultured per single-shot mass spectrometry (MS) replicate, and ~150 million HeLa cells were prepared for each pre-fractionated MS replicate. HeLa cells were either left untreated (control) or treated with 1 mM $H_2O_2$ (Sigma Aldrich) for 10 min in PBS at 37°C with or without prior incubation with the PARP inhibitor Olaparib (10 μM; Selleckchem) for 1 h. Quadruplicate cultures were prepared for all biological conditions. For

western blot (WB) analysis, cells were left untreated or treated with 1 mM $H_2O_2$ for the indicated time points, in medium, and with or without prior incubation with Olaparib for a total of 3 h. All western blot analyses were performed in duplicate.

### Cell lysis and sample preparation

To achieve a high recovery of proteins and avoid loss of biologically labile PTMs, we used a procedure based on lysis with the highly chaotropic agent guanidine-HCl. Cells were washed twice with ice-cold PBS, and harvested by gentle scraping at 4°C. Cells were pelleted by centrifugation, washed with PBS, and re-pelleted. For MS analysis, cells were lysed in 10 volumes of lysis buffer (6 M guanidine-HCl, 50 mM Tris, pH 8.5), and the lysate was immediately snap frozen using liquid nitrogen. For each single-shot MS replicate, ~75 million HeLa cells corresponded to ~15 mg of total protein material. For each pre-fractionated MS replicate, ~150 million HeLa cells corresponded to ~30 mg of total protein material. After thawing, cell lysates were sonicated, and supplemented with 5 mM TCEP and 10 mM chloroacetamide (CAA). The reduced and alkylated proteins were subsequently digested using Lysyl Endopeptidase (Lys-C, 1:100 w/w; Wako Chemicals), and with modified sequencing grade trypsin (1:100 w/w; Sigma Aldrich) after a threefold dilution in 50 mM ammonium bicarbonate. Protease digestion was terminated by addition of trifluoroacetic acid (TFA) to a final concentration of 0.5% (v/v). Precipitates were removed by centrifugation, before peptides were purified using reversed-phase Sep-Pak C18 cartridges (Waters). For WB analysis, cells were lysed in 10 volumes of WB lysis buffer (2% SDS, 150 mM NaCl, 50 mM Tris, pH 8.5), and the lysates were immediately heated to 99°C and shaken at 1,400 RPM for 30 minutes. Temperature-homogenized lysates were equalized for protein concentration using Pierce BCA Protein Assay Kit (Thermo) according to the manufacturer's instructions, and supplemented with ½ volume of 4 × NuPAGE LDS Sample Buffer (Thermo).

### Purification of GST-tagged Af1521 macrodomain

To purify ADP-ribosylated peptides, we utilized a GST-tagged Af1521 macrodomain, which can be readily produced in-house using bacteria (Martello et al., 2016). Competent BL21(DE3) bacteria were used for expression of GST-tagged Af1521. In brief, the plasmid was added to BL21(DE3) on ice, and incubated for 30 min. Bacteria were heat shocked at 42°C for 45 s, incubated on ice, prior to overnight incubation on ampicillin plates. A single colony was inoculated in LB media and grown overnight at 37°C. The starter culture was diluted, and grown to an OD600 of 0.55-0.65. Protein expression was induced by addition of IPTG, for 6 h at 30°C. Bacteria were pelleted by centrifugation, washed twice with PBS, and pellets were frozen at −80°C until further processing. Bacterial pellets were lysed using BugBuster® Protein Extraction Reagent (Merck) according to the manufacturer's instructions. GST-tagged Af1521 was subsequently purified from the bacterial lysate using glutathione Sepharose 4B (Sigma Aldrich), by incubating the beads in the lysate for 4 h at 4°C. Beads were subsequently washed five times with PBS, and then stored until use at 4°C in PBS supplemented with 10 mM sodium azide.

### Enrichment of ADP-ribosylated peptides

To allow identification of ADP-ribosylation on peptides, ADP-ribosylation has to be reduced to monomers using the PARG enzyme, and subsequently purified to a high degree using the Af1521 macrodomain and a considerable number of washing steps. Peptides purified from digested HeLa lysates were eluted off the Sep-Pak cartridges using acetonitrile (ACN) in 0.1% TFA, and dried by vacuum centrifugation at 60°C. Peptides were dissolved in Milli-Q water (MQ), and passed through 0.45 μm filters prior to concentration determination by UV spectroscopy. Peptide amount at this stage was approximately $1/4^{th}$ of the initial total protein amount. Samples were subsequently buffered to achieve final concentrations of 50 mM TRIS pH 8.0, 1 mM $MgCl_2$, 250 μM DTT, and 50 mM NaCl. ADPr-polymer complexity was reduced by incubation with recombinant PARG (a kind gift from Prof. Dr. Michael O. Hottiger) at a concentration of 1:10,000 (w/w, PARG-to-substrate), overnight at 20°C. ADPr-modified peptides were subsequently purified by addition of Sepharose beads with GST-tagged Af1521 macrodomain, and incubation for 3 h at 4°C. The beads were washed four times in ice-cold Wash Buffer (50 mM TRIS pH 8.0, 1 mM $MgCl_2$, 250 μM DTT, 50 mM NaCl), two times in ice-cold PBS, and two times in ice-cold MQ. ADP-ribosylated peptides were eluted off the beads over two rounds using two bead volumes ice-cold 0.15% TFA.

### Enrichment of phosphorylated peptides

To evaluate the phosphoproteome, we used a similar experimental setup as for ADP-ribosylation, and used an established high-efficiency method for purification of phosphopeptides. Quadruplicate HeLa cultures with ~50 million cells were prepared, and treated, lysed, and digested similarly to the HeLa cells prepared for ADP-ribosylation analysis. Trypsin-digested peptides were eluted off Sep-Pak using acetonitrile (ACN) in 0.1% TFA, and all samples were brought to concentrations of 80% ACN and 5% TFA in a final volume of 8 ml. Each sample (3 mg of peptides) was incubated with 1.5 mg of $TiO_2$ beads (GL Sciences) for 30 min at room temperature, followed by a second incubation of the unbound fraction with another 1.5 mg of $TiO_2$ beads. Beads were washed with ACN/TFA on C8 StageTips, prior to elution with $NH_4OH$ (Bekker-Jensen et al., 2017).

### Fractionation of peptides by StageTip

In order to achieve a considerable depth of sequencing, we used high-pH reversed-phase pre-fractionation to distribute the final purified peptides across multiple fractions, with each of these fractions being considerably less complex than a single-shot sample. One third of all ADP-ribosylation samples were acidified by addition of TFA to 1% final volume, and subsequently peptides were

purified and desalted using reversed-phase C18 StageTips (Rappsilber et al., 2003). Two thirds of all ADP-ribosylation samples were supplemented with ammonium hydroxide to a final concentration of 20 mM, and peptides were purified, desalted, and fractionated on-StageTip (Hendriks et al., 2017). ADP-ribosylation samples were eluted as six fractions using 2% (F1), 4% (F2), 7% (F3), 10% (F4), 15% (F5), and 25% (F6) of ACN in 20 mM ammonium hydroxide. Flow-through from the initial loading of the samples at high-pH was acidified and processed on separate StageTips at low-pH, resulting in a seventh fraction (F0). Phosphorylation samples were eluted as six fractions using 2% (F1), 4% (F2), 7% (F3), 10% (F4), 13% (F5), and 25% (F6) of ACN in 20 mM ammonium hydroxide. All peptide elutions were vacuum-dried completely, and dissolved in a small volume of 0.1% formic acid.

### Mass spectrometric analysis

We operated our chromatography equipment and mass spectrometers according to optimized protocols and methodology in order to ensure a maximum degree of sensitivity. All ADP-ribosylation MS experiments were performed using a nanoscale EASY-nLC 1200 system (Thermo) connected to a Fusion Lumos Orbitrap mass spectrometer (Thermo), whereas the phosphorylation MS experiments were performed using a Q Exactive HF-X, both equipped with a nano-electrospray source (Thermo). All samples were analyzed on 15-cm long analytical columns, with an internal diameter of 75 μm, and packed in-house using ReproSil-Pur 120 C18-AQ 1.9 μm beads (Dr. Maisch). Reversed-phase liquid chromatography was performed using an EASY-nLC 1200 system (Thermo). The analytical column was heated to 40°C, and elution of peptides from the column was achieved by application of gradients with Buffer A (0.1% formic acid) and increasing amounts of Buffer B (80% ACN in 0.1% formic acid). For single shot ADP-ribosylation samples, the primary gradient ranged from 4% buffer B to 40% buffer B over 90 minutes, followed by an increase to 55% buffer B to ensure elution of all peptides, followed by a washing block of 20 minutes. For fractionated ADP-ribosylation samples, the gradient ranged from 3% buffer B to 40% buffer B over 62 minutes, followed by a washing block of 18 minutes. For fractionated phosphorylation samples, the gradient ranged from 5% buffer B to 50% buffer B over 82 minutes, followed by a washing block of 18 minutes. Electrospray ionization (ESI) was achieved using a Nanospray Flex Ion Source (Thermo). Spray voltage was set to 2 kV, capillary temperature to 275°C, and RF level to 30% for all ADP-ribosylation samples, and 40% for phosphorylation samples. For ADP-ribosylation samples, full scans were performed at a resolution of 60,000, with a scan range of 300 to 1,750 *m/z*, a maximum injection time of 60 ms, and an automatic gain control (AGC) target of 600,000 charges. Precursors were isolated with a width of 1.3 *m/z*, with an AGC target of 200,000 charges, and precursor fragmentation was accomplished using electron transfer dissociation (ETD) using calibrated charge-dependent ETD parameters. Calibration of ETD was essentially performed as described previously (Rose et al., 2015). The ion trap and the Orbitrap were calibrated and evaluated in negative mode. For ETD, Reagent Transmission, IC Transmission, and Reagent Ion Source were all evaluated on a weekly basis. The internal calibration stored in the instrument resulted in activation times of 110.80 ms for $z = 2$ precursors, 49.24 ms for $z = 3$ precursors, 27.70 ms for $z = 4$ precursors, and 17.73 ms for $z = 5$ precursors. This equates to an ETD Time Constant ($\tau$) of 2.46. Only precursors with charge state 3-5 were considered, and prioritized from charge 3 (highest) to charge 5 (lowest), using the decision tree algorithm. Selected precursors were excluded from repeated sequencing by setting a dynamic exclusion of 72 s for single shot samples, and 48 s for fractionated samples. MS/MS spectra were acquired in the Orbitrap, and settings included a loop count of 5, a maximum injection time of 120 ms and a resolution of 60,000. For phosphorylation samples, full scans were performed at a resolution of 60,000, with a scan range of 300 to 1,500 *m/z*, a maximum injection time of 60 ms, and an automatic gain control (AGC) target of 3e6 charges. Precursors were isolated with a width of 1.3 *m/z*, with an AGC target of 2e5 charges, and precursor fragmentation was accomplished using higher energy collision dissociation (HCD). Only precursors with charge state 2-5 were considered. Selected precursors were excluded from repeated sequencing by setting a dynamic exclusion of 90 s. MS/MS spectra were acquired in the Orbitrap, and settings included a loop count of 9, a maximum injection time of 90 ms and a resolution of 45,000.

### Data analysis

Analysis of the mass spectrometry raw data was performed using the MaxQuant software, which is freely available, routinely used in the field, and one of the best solutions for studying PTMs. An overview detailing which RAW files correspond to which experimental conditions is available (Table S1). For the ADP-ribosylation main search, all corresponding RAW files were analyzed using the freely available MaxQuant software (version 1.5.3.30). Default MaxQuant settings were used, with exceptions outlined below. For generation of the theoretical spectral library, the HUMAN.fasta database was extracted from UniProt on the 23rd of January, 2018. Cysteine carbamidomethylation, N-terminal acetylation, methionine oxidation, and ADP-ribosylation on a wide range of amino acid residues (C, D, E, H, K, R, S, T, and Y) were included as variable modifications. A maximum allowance of 5 variable modifications per peptide was used. Label-free quantification (LFQ) was enabled. Second peptide search was enabled (default), and matching between runs was enabled with a match time window of 1 minute and an alignment time window of 20 minutes. Data was filtered by posterior error probability to achieve a false discovery rate of < 1% (default), at the peptide-spectrum match, the protein assignment, and the site-specific levels. For the ADP-ribosylation unrestricted search, only single-shot RAW files were analyzed with MaxQuant to minimize computational processing time. All other search parameters were the same as for the main search, with exceptions outlined below. For the unrestricted search, ADP-ribosylation was allowed as a variable modification on all 20 naturally occurring amino acids, no other variable modifications were considered, the maximum number of variable modifications per peptide was set to 1, and the maximum peptide mass was set to 2,500. For the phosphorylation main search, up to 8 missed tryptic cleavages were allowed, and a maximum peptide mass of 7,000 Da was set. Protein N-terminal acetylation, methionine oxidation, and

phosphorylation of serine, threonine, and tyrosine residues were included as potential variable modifications. A maximum allowance of 4 variable modifications per peptide was used. Second peptide search was enabled (default), and matching between runs was enabled with a match time window of 1 minute and an alignment time window of 20 minutes. Modified peptides were filtered to have a delta score of at least 20. Data was additionally filtered by posterior error probability to achieve a false discovery rate of < 1% (default), at the peptide-spectrum match, the protein assignment, and the site-specific levels.

### Validation of ADPr on CHTY residues

We performed manual verification for three representative MS/MS spectra corresponding to ADP-ribosylation targeting cysteine, histidine, threonine, or tyrosine residues, because modification of these residues has not previously been demonstrated using MS/MS in combination with ETD fragmentation. The MaxQuant Viewer (integrated in MaxQuant 1.5.3.30) was used to export automatically annotated ETD MS/MS spectra corresponding to peptides ADP-ribosylated on C, H, T, or Y residues, which were manually verified for the presence of mass fragments unequivocally demonstrating correct localization. The annotated spectra are available as Supplemental Data (Data S1).

### Western blot analysis

We utilized western blot analysis to investigate the phosphorylation state of specific proteins of interest. Total HeLa cell lysates were size-separated on 4%–12% Bis-Tris gels using MOPS running buffer, and transferred to PVDF membranes (Millipore). Total protein loading was ensured by Ponceau-S staining. Membranes were blocked using 5% BSA solution in PBS supplemented with 0.1% Tween-20 (PBST) for 1 h. Subsequently, membranes were incubated with primary antibodies overnight at 4°C. Membranes were washed three times with PBST, and incubated with Goat-anti-rabbit HRP conjugated secondary antibody (Jackson Immunoresearch, 111-036-045) at a concentration of 1:2500 for 1 h at room temperature. Membranes were washed three times with PBST prior to detection using Novex ECL Chemiluminescent Substrate Reagent Kit (Invitrogen). The following primary antibodies were used in this study: phospho-Aurora A (Thr288)/Aurora B (Thr232)/Aurora C (Thr198) rabbit mAb, phospho-Histone H3 (Ser10) rabbit mAb, and phospho-TACC3 (Ser558) rabbit mAb (all from Cell Signaling Technology), all diluted 1:1,000 in 5% BSA.

## QUANTIFICATION AND STATISTICAL ANALYSIS

Details regarding the statistical analysis can be found in the respective figure legends. Statistical handling of the data was primarily performed using the freely available Perseus software (Tyanova et al., 2016), and includes $\log_2$ transformations, n = 4 filtering, imputation (down shift 1.8, width 0.3), scatterplot analysis, principle component analysis, Z-scoring, unsupervised hierarchical clustering, and enrichment analysis through FDR-controlled Fisher Exact testing. Protein annotations used for term enrichment analysis, including Gene Ontology, keywords, and Pfam, were concomitantly downloaded from UniProt with the HUMAN.fasta file used for searching the RAW data. The iceLogo software (version 2.1) was used for sequence motif analysis (Colaert et al., 2009). The online Kinase-Substrate Enrichment Application (KSEA) was used for matching kinase motifs to all serines in ADPr-modified proteins (Casado et al., 2013), with kinase motifs extracted from PhosphoSitePlus (Hornbeck et al., 2012) and Networkin (Linding et al., 2007). The online STRING database (version 10.5) was used for generation of protein interaction networks (Szklarczyk et al., 2015), and Cytoscape (version 3.6.0) was used for manual annotation and visualization of the STRING networks (Shannon et al., 2003).

## DATA AND SOFTWARE AVAILABILITY

The accession numbers for the ADP-ribosylation data and the phosphorylation data reported in this paper are ProteomeXchange Consortium PRIDE: PXD009208 and PXD009931, respectively (Vizcaíno et al., 2013).